Statistical properties of a perimeter estimator for spatial excursions observed over regular grids

Ryan Cotsakis, Elena Di Bernardino, Thomas Opitz

STATISTICAL PROPERTIES OF A PERIMETER ESTIMATOR FOR SPATIAL EXCURSIONS OBSERVED OVER REGULAR GRIDS

BY RYAN COTSAKIS[1,*], ELENA DI BERNARDINO[1,†] AND THOMAS OPITZ[2]

[1]*Laboratoire J.A. Dieudonné, Université Côte d'Azur, Nice, France,* [*]*ryan.cotsakis@univ-cotedazur.fr;* [†]*elena.di_bernardino@univ-cotedazur.fr*

[2]*INRAE-BioSP, Avignon, France, thomas.opitz@inrae.fr*

We are interested in creating methods to provide informative summaries of random fields through the geometry of their excursion sets. To this end, we introduce an estimator for the perimeter of excursion sets of random fields. The parsimonious estimator acts on binary digital images of the excursions and computes the length of a piecewise linear approximation of the boundary. Consistency and asymptotic normality results are obtained for decreasing pixel size and growing domain, without the restrictive assumption of isotropy of the underlying random field. We conduct several numerical studies that suggest our asymptotic results are well approximated in the finite data setting.

1. Introduction. Random fields play a central role in the study of many real-world phenomena. In many applications, the excursion set of a random field (*i.e.*, the subset of the domain on which the random field exceeds a certain threshold) is observed—or partially observed—and its geometry can be used to make meaningful inferences about the underlying field. Such techniques have been used in disciplines such as astrophysics, brain imaging, and environmental sciences (Gott et al., 1990; Worsley et al., 1992; Angulo and Madrid, 2010; Lhotka and Kyselỳ, 2015; Frölicher, Fischer and Gruber, 2018). In some cases, for example in landscape ecology, land-use analysis, and statistical modeling, understanding the geometry of excursions is one of the primary objectives (McGarigal, 1995; Nagendra, Munroe and Southworth, 2004; Bolin and Lindgren, 2015).

Geometric summaries of excursion sets, namely Lipschitz-Killing (LK) curvatures, have recently been used for parametric inference (Biermé et al., 2019; Di Bernardino and Duval, 2020) and to test for Gaussianity, isotropy, and marginal symmetry of the underlying fields (Cabaña, 1987; Di Bernardino, Estrade and León, 2017; Berzin, 2017; Abaach, Biermé and Di Bernardino, 2021). Making use of the LK curvatures of excursion sets for statistical inference has the practical advantage that very little information about the underlying field is needed to compute these geometric summaries. To further emphasise their importance, LK curvatures of excursions have deep links to extreme value theory; these insights are summarized in Adler and Taylor (2007) and Azais and Wschebor (2007). LK curvatures can thus provide meaningful and parsimonious summaries of spatial properties of the studied random fields.

In the two-dimensional setting, there are three LK curvatures that can be leveraged to describe excursions of random fields in $\mathbb{R}^2$; that is, the area, half the value of the perimeter, and the Euler-Poincaré characteristic. In practice, data are often provided over regular spatial grids, making the perimeter a particularly difficult quantity to estimate. There exists a number of algorithms for computing the perimeter of objects in digital images, many of which are summarised in Coeurjolly and Klette (2004) with further developments made in de Vieilleville,

MSC2020 subject classifications: 62H11, 62M40, 60G60.

Keywords and phrases: Geometric inference, Excursion sets, Digital geometry, Threshold exceedances.

Lachaud and Feschet (2007). It seems, however, intractable to evaluate the performance of these algorithms on random objects, in particular, excursion sets of two-dimensional random fields. Biermé and Desolneux (2021) studies how the integrated perimeter of excursion sets over a set of levels changes when considering discretized versions of the underlying stationary, isotropic random fields (*i.e.*, those with translation- and rotation-invariant distributions). This gives rise to a perimeter estimator complete with its own probabilistic analysis that Abaach, Biermé and Di Bernardino (2021) expands on.

We introduce a class of estimators for the perimeter of objects in binary digital images, suitable for estimating the perimeter of excursion sets of random fields on $\mathbb{R}^2$. The elements of the class are uniquely associated to the choice of norm that is used to measure a piecewise linear approximation of the excursion's boundary. The estimator derived from the work of Biermé and Desolneux (2021) arises as the element of the proposed class associated to the 1-norm. The novel estimator associated to the 2-norm (the primary focus of this paper) possesses the desirable property of so-called multigrid convergence (*i.e.*, strong consistency as the pixel size tends to zero; see Theorem 1), which we extend to convergence in mean (see Proposition 1). These are general results that hold without the restrictive assumptions of isotropy or Gaussianity of the underlying random field. In the Gaussian framework, we show that the estimator built on the 2-norm is asymptotically normal with the same asymptotic variance as the perimeter itself (see Theorem 2). This known variance can be written in terms of a polynomial chaos expansion (see Theorem 3 in Kratz and León (2001)).

The organisation of the paper is as follows. Section 2 specifies the notion of an excursion set, the assumptions on the underlying random fields, the regular grid on which the excursion sets are observed, and the novel class of perimeter estimators. In Section 3, the statistical properties of the perimeter estimator based on the 2-norm are discussed. Section 4 provides extensive numerical results to support and illustrate the theory developed in Section 3. A useful theoretical result is included in Section 4.3, which provides an explicit formula for the expected perimeter of the excursion sets of some geometrically anisotropic random fields (see Proposition 3). Proofs and auxiliary notions are postponed to Section 5.

2. Definitions and Notation. Let us begin by introducing some notation. Calligraphic font is used to denote sets of isolated points in $\mathbb{R}^2$. For a set $S \subset \mathbb{R}^2$, its boundary is denoted $\partial(S)$; its cardinality $\#(S)$; and its Lebesgue measure $\nu(S)$. We use $\mathcal{H}^1$ to denote the one-dimensional Hausdorff measure, and C^k to denote the space of functions on $\mathbb{R}^2$ with k continuous derivatives. Between the nomenclatures *sample paths* and *trajectories*, we choose to use the former when describing the realizations of a random field.

The following assumption ensures that the random objects that we consider are well defined.

ASSUMPTION 1. The real-valued stationary random field $X = \{X(s) : s \in \mathbb{R}^2\}$ defined on a probability space $(\Omega, \mathcal{F}, \mathbb{P})$ has C^2 sample paths.

DEFINITION 1 (Excursion set). Denote the *excursion set* of X at the level $u \in \mathbb{R}$ by $E_X(u) := \{s \in \mathbb{R}^2 : X(s) \geq u\}$. For compact $T \subset \mathbb{R}^2$, we denote the restriction of $E_X(u)$ and $\partial\big(E_X(u)\big)$ to T by

$$E_X(T,u) := T \cap E_X(u) \qquad \text{and} \qquad E_X^{\partial}(T,u) := T \cap \partial\big(E_X(u)\big)$$

respectively. Finally, the quantity of interest in this paper is

$$P_X^T(u) := \mathcal{H}^1\big(E_X^{\partial}(T,u)\big).$$

In Figure 1 (a), a sample path of an isotropic, Gaussian random field X is depicted in a square domain T with the contours $E_X^{\partial}(T,u)$ drawn on the domain for various levels u. In Figure 1 (b) and (c), $E_X(u)$ is represented by the dark regions, for two different levels u.

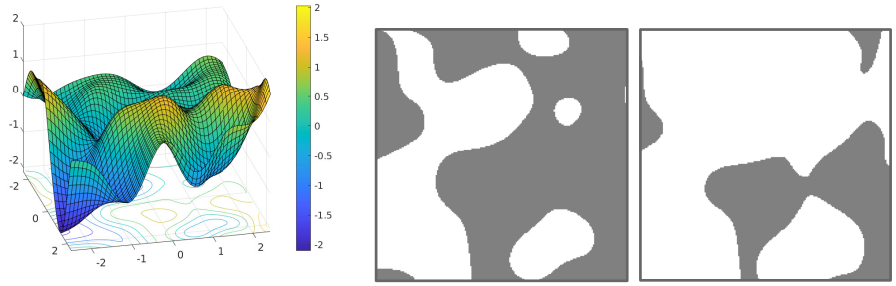

(a) (b) (c)

Fig 1: (a) A realization of a stationary random field X with standard Gaussian margins and covariance function $R(h) = \exp(-||h||_2^2)$ is depicted in the square-shaped observation window $T = [-2.5, 2.5]^2$ (generated using the R package `RandomFields`). Underneath the field are the curves $E_X^{\partial}(T,u)$ for different values of u. (b) (resp. (c)) The dark region $E_X(T,u)$ is shown for $u = 0$ (resp. $u = 0.5$).

In what follows, let

$$T := [-t,t]^2 \subset \mathbb{R}^2, \tag{1}$$

for fixed $t > 0$. Before proceeding, it is helpful to specify additional assumptions on the considered random fields.

ASSUMPTION 2. Let X_1 and X_2 denote the partial derivatives of X in the two principle Cartesian directions in $\mathbb{R}^2$, and let X_{11} and X_{22} denote the corresponding second order partials. For any $u \in \mathbb{R}$, the following three conditions hold almost surely:

1. X has no critical points in T at the level u.
2. The restriction of X to each face of the square boundary $\partial(T)$ has no local extrema at the level u.
3. For $k \in \{1,2\}$, there are no $s \in T$ such that $X(s) - u = X_k(s) = X_{kk}(s) = 0$.

The random fields that satisfy Assumptions 1 and 2 are almost surely *suitably regular* at the level u in T as defined in Adler and Taylor (2007, Definition 6.2.1) which is useful when considering the set

$$\mathcal{Y}_X^T(u) := \bigcup_{k=1,2} \{s \in E_X^{\partial}(T,u) : X_k(s) = 0\}. \tag{2}$$

Indeed, under Assumptions 1 and 2, it follows directly from Adler and Taylor (2007, Lemma 6.2.3) that

$$\#\big(\mathcal{Y}_X^T(u)\big) < \infty \qquad a.s. \tag{3}$$

Recall that the *reach* of a set $S \subset \mathbb{R}^d$ is given by

$$\operatorname{reach}(S) := \sup\{\delta \geq 0 : \forall y \in S_\delta \; \exists! x \in S \text{ nearest to } y\}, \tag{4}$$

where $S_\delta = \{y \in \mathbb{R}^d : \exists\, x \in S \text{ s.t. } ||x-y||_2 \leq \delta\}$ is the dilation of the set S by a radius $\delta \geq 0$ (see, *e.g.*, Definition 11 in Thäle (2008)). Equations (3) and (4) will be useful later (see, for example, Remark 4).
Recall that a curve $\gamma \subset \mathbb{R}^2$ is connected if it cannot be expressed as the union of two disjoint nonempty closed sets in $\mathbb{R}^2$. For sets $B \subseteq A \subseteq \mathbb{R}^2$, B is maximally connected in A if B is connected and there does not exist a connected $C \subseteq A$ such that $B \subset C$.

DEFINITION 2. Let $\Gamma_X^T(u)$ be the set of maximally connected subsets of $E_X^\partial(T,u)$.

ASSUMPTION 3. The random variables $P_X^T(u)$ and $\#\big(\Gamma_X^T(u)\big)$ are in $L^1(\Omega)$ for all $u \in \mathbb{R}$.

We emphasise that none of the assumptions introduced in this section restrict to isotropic random fields. Therefore, our results are applicable to anisotropic random fields—a crucial point that we investigate in Section 4.3.
In what follows, we study a novel estimator of the random quantity $P_X^T(u)$ for arbitrary but fixed $u \in \mathbb{R}$, based only on the random field $Z_X(\cdot;u) = \{Z_X(s;u) : s \in \mathbb{R}^2\}$ defined by

$$Z_X(s;u) := \mathbb{1}_{\{s \in E_X(u)\}} = \mathbb{1}_{\{X(s) \geq u\}}, \qquad s \in \mathbb{R}^2.$$

Note that Z_X has dependent Bernoulli margins with parameter $\mathbb{P}\big(X(0) \geq u\big)$.

2.1. *Sampling locations on a regular grid.* The process Z_X is evaluated at sampling locations on the regular grid defined as follows.

DEFINITION 3 (Square grid). Fix $\epsilon > 0$, and define a square grid of points in $\mathbb{R}^2$ as

$$\mathcal{G}^{(T,\epsilon)} := \big\{s_{i,j} : i,j \in \mathbb{N}_0\big\} \cap T, \tag{5}$$

with

$$s_{i,j} := (-t + i\epsilon, -t + j\epsilon) \in \mathbb{R}^2,$$

and with T and t as in Equation (1). Let M be the number of rows (which is identical to the number of columns) of $\mathcal{G}^{(T,\epsilon)}$. Define the index set

$$I^{(T,\epsilon)} := \{0, \ldots, M-1\} \subset \mathbb{N}_0$$

and the random matrix $\zeta_X^{(T,\epsilon)}(u)$ with binary elements

$$\zeta_{X,i,j}^{(T,\epsilon)}(u) := Z_X(s_{i,j};u) = \mathbb{1}_{\{X(s_{i,j}) \geq u\}}, \qquad i,j \in I^{(T,\epsilon)}. \tag{6}$$

For $m \in \mathbb{N}^+$, let us define

$$I^{(T,\epsilon,m)} := \{i \in I^{(T,\epsilon)} : i \equiv 0 \pmod m\}.$$

Notice that $\mathcal{G}^{(T,\epsilon)} = \{s_{i,j} : i,j \in I^{(T,\epsilon)}\}$. We provide an illustration of $\mathcal{G}^{(T,\epsilon)}$ in Figure 2, where the elements with indices in $I^{(T,\epsilon,m)}$ are highlighted in red.

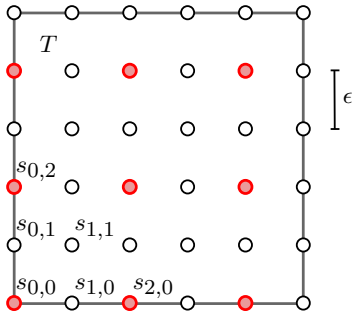

Fig 2: An illustration of the quantities defined in Definition 3. The positions of the elements of $\mathcal{G}^{(T,\epsilon)}$ in $\mathbb{R}^2$ are shown as circles, and the subset $\{s_{i,j} : i,j \in I^{(T,\epsilon,m)}\}$ with $m = 2$ is highlighted in red. Here, $M = 6$, and the side length of T is $\sqrt{\nu(T)} = (M-1)\epsilon = 5\epsilon$.

REMARK 1. The data matrix $\zeta_X^{(T,\epsilon)}(u)$ in (6) can be represented as a binary digital image as depicted in Figure 3 (b). In this framework, M corresponds to the pixel density or grid size of the image (an integer number of pixels per distance of $2t$, the side length of T), and ϵ corresponds to the pixel width. The quantities are related by $|M\epsilon - 2t| \leq \epsilon$.

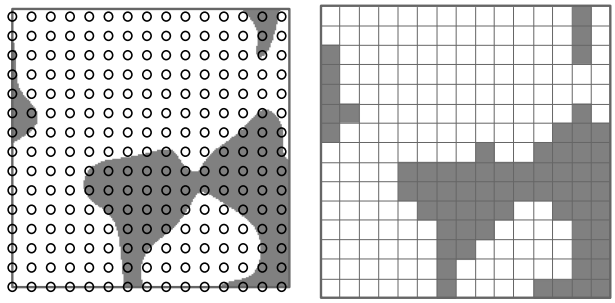

(a) (b)

Fig 3: (a) $E_X(T, 0.5)$, as shown in Figure 1 (c), superposed with the elements of the grid $\mathcal{G}^{(T,\epsilon)}$ shown as black circles. Here, $\epsilon \approx 0.32$. (b) The binary matrix $\zeta_X^{(T,\epsilon)}(0.5)$, defined in (6), represented as a binary digital image (dark pixels corresponding to 1, and white to 0).

2.2. *Definition of the estimators.* Here, we introduce a class of estimators of $P_X^T(u)$ that use only the information contained in $\zeta_X^{(T,\epsilon)}(u)$, defined in (6). We separate $\zeta_X^{(T,\epsilon)}(u)$ into submatrices, and in each submatrix we compute the length of the line segment that approximately separates the 1's from the 0's. In this way, the estimator obtained depends on the choice of norm used.

DEFINITION 4 (Perimeter estimator). With $||\cdot||_p$ denoting the p-norm, define

(7)
$$\hat{P}_X^{(p)}(\epsilon, m; T, u) := \epsilon \sum_{a \in I^{(T,\epsilon,m)}} \sum_{b \in I^{(T,\epsilon,m)}} \left|\left|\left(N_{X,h}(a,b;u), N_{X,v}(a,b;u)\right)\right|\right|_p, \qquad p \in \mathbb{N}^+,$$

where

$$N_{X,h}(a,b;u) := \sum_{i=a}^{a+m-1\wedge M-1} \sum_{j=b}^{b+m-1\wedge M-2} |\zeta_{X,i,j}^{(T,\epsilon)}(u) - \zeta_{X,i,j+1}^{(T,\epsilon)}(u)|, \qquad a,b \in I^{(T,\epsilon,m)},$$

and

$$N_{X,v}(a,b;u) := \sum_{i=a}^{a+m-1\wedge M-2} \sum_{j=b}^{b+m-1\wedge M-1} |\zeta_{X,i,j}^{(T,\epsilon)}(u) - \zeta_{X,i+1,j}^{(T,\epsilon)}(u)|, \qquad a,b \in I^{(T,\epsilon,m)}.$$

Figure 4 illustrates the behavior of the estimator in Equation (7) constructed with two different norms, *i.e.*, with $p = 1$ and $p = 2$.

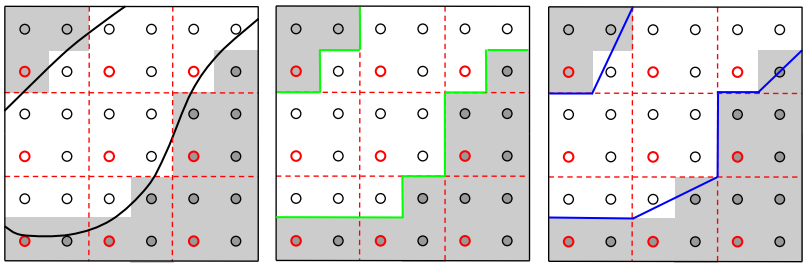

(a) (b) (c)

Fig 4: (a) The curve $E_X^{\partial}(T,u)$ is shown in relation to the points in $\mathcal{G}^{(T,\epsilon)}$. Points in the dark regions are assigned a value of 1 in the matrix $\zeta_X^{(T,\epsilon)}(u)$, and points in white are assigned a value of 0. The points outlined in red have indices in $I^{(T,\epsilon,m)}$ with $m = 2$. In effect, $\hat{P}_X^{(1)}(\epsilon,2;T,u)$ is calculated by counting the pixel edges shown in green (see panel (b)), whereas $\hat{P}_X^{(2)}(\epsilon,2;T,u)$ is calculated by summing the lengths of the blue piecewise linear curves (see panel (c)).

Continuing from the framework discussed in Remark 1, $N_{X,v}$ (resp. $N_{X,h}$) counts the number of pixels in a subrectangle—of size at most $m \times m$ pixels—of T that differ in shade from the neighbouring pixel to the right (resp. above). In other words, $N_{X,v}$ (resp. $N_{X,h}$) provides a count of significant vertical (resp. horizontal) pixel edges in the subrectangle.
By considering the estimator in (7) with norm $p = 1$, one recovers the estimator that is extensively studied in Biermé and Desolneux (2021). It counts the number of pixel edges that separate pixels of different color, and rescales the count by ϵ (see Figure 4 (b)). Thus, $\hat{P}_X^{(1)}(\epsilon,m;T,u)$ will not depend on m, so we write $\hat{P}_X^{(1)}(\epsilon;T,u)$ in place of $\hat{P}_X^{(1)}(\epsilon,m;T,u)$. The estimator in (7) with norm $p = 2$ approximates the length of $E_X^{\partial}(T,u)$ by the total length of a set of line segments that approximate the curve (see Figure 4 (c)). The hyperparameter m is related to the number of line segments used to approximate $E_X^{\partial}(T,u)$, and so $\hat{P}_X^{(2)}(\epsilon,m;T,u)$ depends on m. We provide an adaptive method to select this hyperparameter in Section 4.4.

3. Main Results. The focus of this section is to prove convergence results for the estimator $\hat{P}_X^{(2)}(\epsilon,m;T,u)$ as $\epsilon \to 0$ and $m \to \infty$. The analysis is separated into two regimes. In Section 3.1, we consider the domain T to be fixed and decrease the pixel width. In Section 3.2, we study the behaviour of the estimator on a sequence of domains that grow to cover $\mathbb{R}^2$ and conclude with a multivariate central limit theorem for the case when multiple levels $(u_1,\ldots,u_k)$ are considered simultaneously.

3.1. *On a fixed domain with decreasing pixel width.* Here, we are interested in the behaviour of the estimator $\hat{P}_X^{(2)}(\epsilon, m; T, u)$ in the case where the domain $T = [-t, t]^2$ is fixed, and the spacing between the locations of the observations in the matrix $\zeta_X^{(T,\epsilon)}(u)$ tends to 0. We proceed to show that the resulting perimeter estimate converges almost surely to $P_X^T(u)$ and give the rate of convergence.

THEOREM 1 (Almost sure consistency). *Let $(m_n)_{n\geq 1}$ be a non-decreasing sequence in $\mathbb{N}^+$ tending to ∞ as $n \to \infty$. Let $(\epsilon_n)_{n\geq 1}$ be a sequence in $\mathbb{R}^+$ such that $m_n \epsilon_n^{2/3}$ converges to a constant $C \in \mathbb{R}^+$ and that the vertices of T are contained in $\mathcal{G}^{(T,\epsilon_n)}$ for all $n \in \mathbb{N}^+$. Then, under Assumptions 1 and 2, for fixed $u \in \mathbb{R}$, it holds that*

$$g_n \left| \hat{P}_X^{(2)}(\epsilon_n, m_n; T, u) - P_X^T(u) \right| \xrightarrow{\text{a.s.}} 0, \qquad n \to \infty,$$

where $(g_n)_{n\geq 1}$ is any non-decreasing sequence such that $g_n = o(m_n)$.

The proof of Theorem 1 is postponed to Section 5.

REMARK 2. Theorem 1 is a statement about the *multigrid convergence* (see for instance Definition 2 of Coeurjolly and Klette (2004)) of $\hat{P}_X^{(2)}(\epsilon_n, m_n; T, u)$ to $P_X^T(u)$ as $n \to \infty$ for almost all sample paths of the random field X. Unsurprisingly, the *speed* of this convergence is $O(1/m_n)$.

Theorem 1 requires that the vertices of T are in $\mathcal{G}^{(T,\epsilon_n)}$ for all $n \in \mathbb{N}^+$, for example as depicted in Figure 2. This prevents the possibility of there being long segments of $E_X^{\partial}(T, u)$ that remain close to the border of T so as to not pass between elements of $\mathcal{G}^{(T,\epsilon_n)}$. In addition, it is supposed that the sequence $(m_n)_{n\geq 1}$ is asymptotically equivalent to $(\epsilon_n^{-2/3})_{n\geq 1}$, which gives the fastest possible rate of convergence of $\hat{P}_X^{(2)}(\epsilon_n, m_n; T, u)$ to $P_X^T(u)$. By relaxing this condition, we obtain the following corollary.

COROLLARY 1. *Under the conditions of Theorem 1, if the requirement that $m_n \epsilon_n^{2/3} \to C$ is relaxed to $m_n \epsilon_n \to 0$, it holds that*

$$\hat{P}_X^{(2)}(\epsilon_n, m_n; T, u) \xrightarrow{\text{a.s.}} P_X^T(u), \qquad n \to \infty.$$

The proof is postponed to Section 5. The following proposition shows that convergence in $L^1(\Omega)$ holds under slightly stronger assumptions. The proof can also be found in Section 5.

PROPOSITION 1. *Let $(m_n)_{n\geq 1}$ be a non-decreasing sequence in $\mathbb{N}^+$ tending to ∞ as $n \to \infty$. Let $(\epsilon_n)_{n\geq 1}$ be a sequence in $\mathbb{R}^+$ such that $m_n \epsilon_n \to 0$ as $n \to \infty$, and that the vertices of T are contained in $\mathcal{G}^{(T,\epsilon_n)}$ for all $n \in \mathbb{N}^+$. Then under Assumptions 1, 2, and 3,*

$$\left| \hat{P}_X^{(2)}(\epsilon_n, m_n; T, u) - P_X^T(u) \right| \xrightarrow{L^1} 0, \qquad n \to \infty,$$

for any fixed $u \in \mathbb{R}$.

REMARK 3. It is shown in Proposition 5 of Biermé and Desolneux (2021) that for a random field X satisfying Assumption 1, if, in addition, X is Gaussian, isotropic, and the supremum of the first and second order partial derivatives of X in the domain T are in $L^1(\Omega)$, then

$$\mathbb{E}[\hat{P}_X^{(1)}(\epsilon; T, u)] \to \frac{4}{\pi} \mathbb{E}[P_X^T(u)], \tag{8}$$

as $\epsilon \to 0$. Proposition 1 is a stronger result under weaker assumptions on X. It implies that

$$\mathbb{E}[\hat{P}_X^{(2)}(\epsilon, m; T, u)] \to \mathbb{E}[P_X^T(u)],$$

as $\epsilon \to 0$ and $m \to \infty$ under the constraint $m\epsilon \to 0$. Thus, the estimator $\hat{P}_X^{(2)}(\epsilon, m; T, u)$ does not suffer from the bias factor of $4/\pi$.

3.2. *On a growing domain with decreasing pixel width.* Consider the sequence $(T_n)_{n\geq 1}$, where

$$T_n := \{ns : s \in T\}$$

is a dilation of the fixed domain $T = [-t, t]^2$. The side length of the square domain T_n is then $2tn$. To prove the consistency of our perimeter estimator when the domain grows to cover $\mathbb{R}^2$, we define *resolution* in the context of excursion sets of random fields, inspired by the notion of optical resolution.

DEFINITION 5 (Resolution). Define the random variable

$$\Lambda_X^T(u) := \min\Big\{\mathrm{reach}\big(E_X(T,u)\big),\ \mathrm{reach}\big(T \setminus E_X(u)\big),\ \mathrm{reach}\big(\mathcal{Y}_X^T(u)\big)\Big\}.$$

For $\lambda \in \mathbb{R}^+$, we say that " $E_X(u)$ *is resolved by* λ *in* T " whenever the random event $\{\lambda < \Lambda_X^T(u)\}$ occurs.

This makes $\Lambda_X^T(u)$ a random geometrical description of $E_X(u)$ in the domain T: $\Lambda_X^T(u)$ is the supremum of the set of $\lambda \in \mathbb{R}^+$ such that one can roll a ball of radius λ along both sides of the curve $E_X^\partial(T, u)$, and that the distances between points in $\mathcal{Y}_X^T(u)$ are all at least 2λ. Figure 5 clarifies some of the notions introduced in Definition 5.

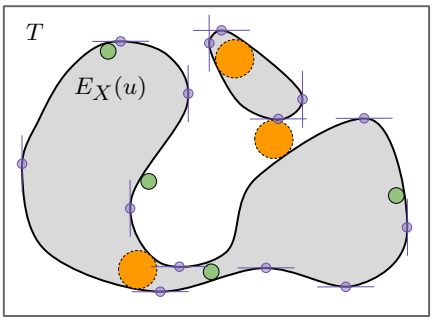

Fig 5: Illustration of the notions of reach and resolution. The reach of $E_X(T, u)$ is greater than the radius, r_{green}, of the small green circles with solid border. The reach of $T \setminus E_X(u)$ is also greater than r_{green}. Moreover, the minimum distance between points in $\mathcal{Y}_X^T(u)$, highlighted in purple, exceeds $2r_{\text{green}}$. Therefore, $E_X(u)$ is *resolved* by r_{green} in T (see Definition 5). Conversely, it is clear that $E_X(u)$ is not resolved in T by the radius of the larger orange circles with dashed border.

REMARK 4. Under Assumptions 1 and 2, the random sets $E_X(T, u)$ and $T \setminus E_X(u)$ have positive reach almost surely, since $E_X(u)$ and $E_{-X}(u)$ are almost surely C^2 submanifolds of $\mathbb{R}^2$ for all $u \in \mathbb{R}$. The intersection of these sets with the compact rectangle T guarantees that the reach of each is positive (Biermé et al., 2019, p. 541). The minimum distance between

points in $\mathcal{Y}_X^T(u)$ is positive by Equation (3) and the compactness of T. Therefore, $\Lambda_X^T(u)$ (see Definition 5) is almost surely positive for all $u \in \mathbb{R}$. It follows that for any $u \in \mathbb{R}$,

$$\mathbb{P}\big(\liminf_{\lambda \to 0} \{\lambda < \Lambda_X^T(u)\}\big) = 1,$$

i.e., with probability 1, there exists a sufficiently small positive λ that resolves $E_X(u)$ in T.

Now that we have defined a number of important quantities for a large class of random fields, we strengthen our hypotheses to the Gaussian framework, and make the following assumption on the random field X.

ASSUMPTION 4 (Kratz and Vadlamani (2018)). Suppose that X is a stationary Gaussian random field with zero-mean, unit-variance, and C^3 sample paths. Define the random field $\mathbf{Y} := (X, X_1, X_2, X_{11}, X_{22}, X_{12})$ with values in $\mathbb{R}^6$, whose components are the partial derivatives of X as indicated by the subscripts. Denote the covariance function of $\mathbf{Y}$ by $R(h) := \big(r_{ij}(h)\big)_{1 \le i,j \le 6}$, with $r_{ij}(h) = \mathrm{Cov}\big(Y_i(0), Y_j(h)\big)$ for $h \in \mathbb{R}^2$. We require that $\max_{1 \le i,j \le 6} \big|r_{ij}(h)\big|$ can be bounded above everywhere on $\mathbb{R}^2$ by an integrable function ψ which satisfies $\psi(h) \to 0$, as $||h||_2 \to \infty$. Finally, assume that for any $h \in \mathbb{R}^2$, the covariance matrix $R(h)$ has full rank.

LEMMA 1. *Assumption 4 implies that Assumptions 1, 2, and 3 are all satisfied.*

PROPOSITION 2. *Let X be a random field satisfying Assumption 4. Let $(m_n)_{n \ge 1}$ be a non-decreasing sequence in $\mathbb{N}^+$ such that $m_n/n \to \infty$. Let $(\epsilon_n)_{n \ge 1}$ be a non-increasing sequence in $\mathbb{R}^+$ satisfying $\epsilon_n = O\big(m_n^{-3/2}\big)$. Moreover, suppose that $2t$ is an integer multiple of ϵ_n for all $n \in \mathbb{N}^+$, and $\mathbb{P}\big(m_n\epsilon_n < \Lambda_X^{T_n}(u)\big) \to 1$ as $n \to \infty$. Then for any $u \in \mathbb{R}$,*

$$\frac{\hat{P}_X^{(2)}(\epsilon_n, m_n; T_n, u) - P_X^{T_n}(u)}{\sqrt{\nu(T_n)}} \xrightarrow{\mathbb{P}} 0,$$

as $n \to \infty$.

The proofs of Lemma 1 and Proposition 2 are postponed to Section 5.

REMARK 5. One example of a sequence $(\epsilon_n)_{n \ge 1}$ satisfying the constraints in Proposition 2 is constructed by letting ϵ_n be the largest element in the sequence $(2t/k)_{k \ge 1}$ such that $\epsilon_n \le m_n^{-3/2}$ and $\mathbb{P}\big(\Lambda_X^{T_n}(u) \le m_n\epsilon_n\big) \le 1/n$, where $\Lambda_X^{T_n}(u)$ is defined in Definition 5. Such a sequence $(\epsilon_n)_{n \ge 1}$ exists since $\mathbb{P}(\Lambda_X^{T_n}(u) \le 0) = 0$ for all $n \in \mathbb{N}^+$ as discussed in Remark 4. The idea is to have the sequence $\lambda_n := m_n\epsilon_n$ tend to 0 faster than the quantiles of $\Lambda_X^{T_n}(u)$, which is difficult to verify analytically. However, in practice, for a given realization of $E_X(u)$, one can estimate $\Lambda_X^T(u)$ by first estimating the reach of the sets $E_X(T, u)$ and $T \setminus E_X(u)$ (see, *e.g.*, Aamari et al. (2019)) and the vector coordinates of the points in $\mathcal{Y}_X^T(u)$, defined in (2).

By leveraging Proposition 2, we prove the multivariate central limit theorem for our estimator as stated in Theorem 2.

THEOREM 2 (CLT for multiple levels). *Let X be a random field satisfying Assumption 4. Let $k \in \mathbb{N}^+$ and fix the vector $\mathbf{u} := (u_1, \ldots, u_k) \in \mathbb{R}^k$ such that $u_i \ne u_j$ for $1 \le i < j \le k$.*

Let the sequences $(m_n)_{n\geq 1}$ and $(\epsilon_n)_{n\geq 1}$ satisfy the constraints detailed in Proposition 2 for all u_j, where $j = 1, \ldots, k$. If we define

$$\hat{P}_X^{(2)}(\epsilon_n, m_n; T_n, \mathbf{u}) := \big(\hat{P}_X^{(2)}(\epsilon_n, m_n; T_n, u_1), \ldots, \hat{P}_X^{(2)}(\epsilon_n, m_n; T_n, u_k)\big)$$

and

$$P_X^{T_n}(\mathbf{u}) := \big(P_X^{T_n}(u_1), \ldots, P_X^{T_n}(u_k)\big),$$

then there exists a finite, non-degenerate (i.e., full-rank) covariance matrix $\Sigma(\mathbf{u})$ such that

$$\frac{\hat{P}_X^{(2)}(\epsilon_n, m_n; T_n, \mathbf{u}) - \mathbb{E}[P_X^{T_n}(\mathbf{u})]}{\sqrt{\nu(T_n)}} \xrightarrow{\mathrm{d}} \mathcal{N}_k\big(\mathbf{0}, \Sigma(\mathbf{u})\big), \qquad n \to \infty.$$

The appropriately rescaled limiting distribution of $P_X^{T_n}(\mathbf{u})$ also has covariance matrix $\Sigma(\mathbf{u})$, which is discussed in Kratz and León (2001). The proof of Theorem 2 is postponed to Section 5.

4. Simulation studies. In this section, we illustrate finite sample performances of our estimator $\hat{P}_X^{(2)}(\epsilon, m; T, \mathbf{u})$ on simulated data. Namely, we wish to showcase the results of Proposition 1 and Theorem 2, and to illustrate the adaptability of the estimator to anisotropic random fields.

4.1. *Convergence in mean in the isotropic case.* Firstly, let us consider the following example.

EXAMPLE 1. Let X be a stationary, isotropic, Gaussian random field on $\mathbb{R}^2$ with zero-mean and unit-variance. The covariance function of X is given by $R(h) = \exp(-||h||_2^2)$ for $h \in \mathbb{R}^2$.

We use the R package `RandomFields` to generate such a random field at the sampling locations in $\mathcal{G}^{(T,\epsilon)}$, with $T = [-2.5, 2.5]^2$. Let $\lfloor \cdot \rfloor$ denote the floor function. For $n \in \mathbb{N}^+$, let

$$M_n = \lfloor 10n^{3/2} \rfloor, \qquad m_n = n, \qquad \text{and} \qquad \epsilon_n = 5/M_n. \tag{9}$$

As noted in Remark 1, the quantity M_n should be interpreted as the pixel density of the discretized domain T, and ϵ_n should be understood as the corresponding pixel width. Figure 6 provides two illustrations of $E_X(u)$, with $u = 0.5$ in the domain T; one containing $M_2 \times M_2$ pixels, and another containing of $M_3 \times M_3$ pixels.

We wish to show numerically that $\hat{P}_X^{(2)}(\epsilon_n, m_n; T, 0.5) \xrightarrow{L^1} P_X^T(0.5)$ as $n \to \infty$. However, there is no way of accessing $P_{X(\omega)}^T(0.5)$ for any realisation $X(\omega)$, so we use a proxy for $P_{X(\omega)}^T(0.5)$ to measure the performance of of our estimator. In Appendix B of Biermé and Desolneux (2021), the authors introduce an estimator that they show converges to $P_X^T(u)$ for any $u \in \mathbb{R}$. For a pixel width of ϵ, denote this estimator by $\tilde{P}_X(\epsilon; T, u)$. Convergence of $\tilde{P}_X(\epsilon_n; T, u)$ to $P_X^T(u)$ in $L^1(\Omega)$ follows from the same arguments that we use in the proof of our Proposition 1. Therefore, for any sequence $(h_n)_{n\geq 1}$,

$$\big|h_n - \tilde{P}_X(\epsilon_n; T, u)\big| \xrightarrow{L^1} 0 \iff h_n \xrightarrow{L^1} P_X^T(u) \tag{10}$$

as $n \to \infty$. The estimator $\tilde{P}_X(\epsilon; T, u)$ takes as its arguments the values of X evaluated on a regular grid, which is precisely the output of the simulation from the `RandomFields` package. Therefore, we are in a position to illustrate the left-hand side of Equation (10) numerically with $h_n = \hat{P}_X^{(2)}(\epsilon_n, m_n; T, u)$.

Figure 6 shows how the mean absolute error (MAE) of the approximation of $\tilde{P}_X(\epsilon_n; T, 0.5)$ (the proxy for $P_X^T(0.5)$) by the estimator $\hat{P}_X^{(2)}(\epsilon_n, m_n; T, 0.5)$ (shown in blue) approaches 0 as $n \to \infty$. The MAE of the approximation of $\tilde{P}_X(\epsilon_n; T, 0.5)$ by $\hat{P}_X^{(1)}(\epsilon_n; T, 0.5)$ (shown in green) tends to a positive value, so by (10), $\frac{\pi}{4}\hat{P}_X^{(1)}(\epsilon_n; T, 0.5)$ does not converge to $P_X^T(0.5)$ in $L^1(\Omega)$ (the interested reader is referred for instance to Theorem 3 in Biermé and Desolneux (2021)), even though $\mathbb{E}\big[\frac{\pi}{4}\hat{P}_X^{(1)}(\epsilon_n; T, 0.5)\big] \to \mathbb{E}\big[P_X^T(0.5)\big]$ as $n \to \infty$ (see Equation (8)).

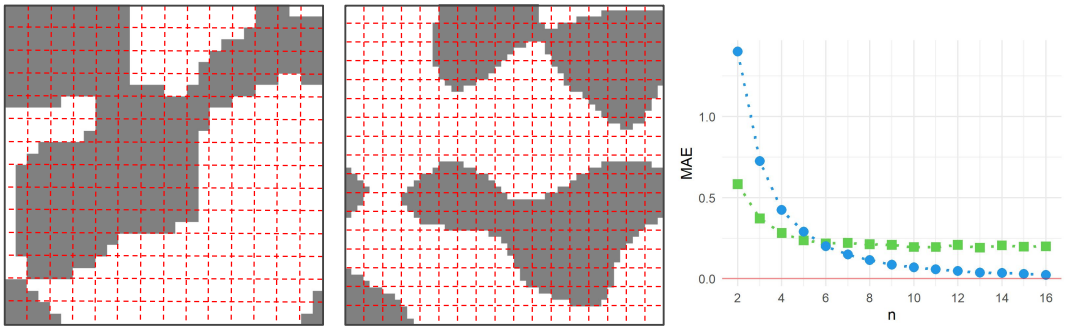

(a) $n = 2$ (b) $n = 3$ (c)

Fig 6: Independent realizations of $E_X(0.5)$ shown in $T = [-2.5, 2.5]^2$, where X is given by Example 1 and M_n, m_n, and ϵ_n are given in (9). (a) The excursion set (shown as the dark region) is generated using $M_2 \times M_2$ pixels, and the dashed red lines have a spacing of $2\epsilon_2$, where ϵ_2 is the pixel width. (b) Here, the size of the image (measured in pixels) is $M_3 \times M_3$, and the dashed red lines have a spacing of $3\epsilon_3$, where ϵ_3 is the pixel width. (c) The approximation of $\tilde{P}_X(\epsilon_n; T, 0.5)$ by $\frac{\pi}{4}\hat{P}_X^{(1)}(\epsilon_n; T, 0.5)$ (green squares) and by $\hat{P}_X^{(2)}(\epsilon_n, m_n; T, 0.5)$ (blue circles) for different values of n. For each n, the MAE of the approximations are calculated from 500 independent replications of the process X. For reference, $\mathbb{E}[P_X^T(0.5)] = 15.6$ (computed via Adler and Taylor (2007, Theorem 15.9.5)).

4.2. *Central limit theorem in the isotropic Gaussian case.* To illustrate Theorem 2, we compute $\hat{P}_X^{(2)}(\epsilon, m; T, \mathbf{u})$ in a large domain $T = [-15, 15]^2$ divided into 1024×1024 pixels, with $m = 8$ and $\mathbf{u} = (0, 0.25, 0.5)$. Again, we consider the random field X from Example 1. Figure 7 shows how the distribution of the random vector $\hat{P}_X^{(2)}(\epsilon, m; T, \mathbf{u})$ is close to a 3-variate normal distribution with mean $\mathbb{E}[P_X^T(\mathbf{u})] = (636, 617, 562)$ (computed via Adler and Taylor (2007, Theorem 15.9.5)).

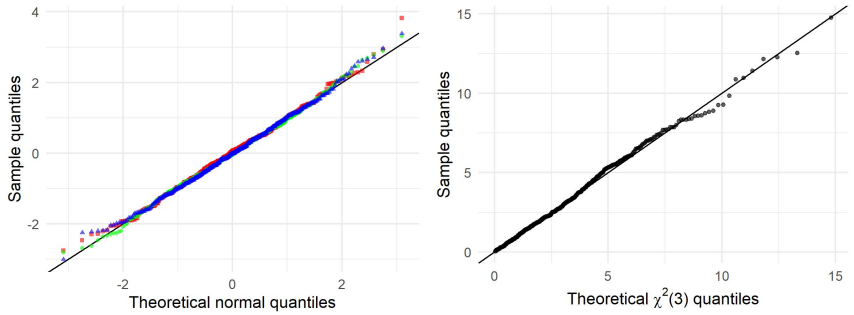

(a) (b)

Fig 7: Illustration of asymptotic normality. We simulated 500 independent replications of the vector $\hat{P}_X^{(2)}(\epsilon, m; T, \mathbf{u})$. (a) The margins of $\hat{P}_X^{(2)}(\epsilon, m; T, \mathbf{u}) - \mathbb{E}[P_X^T(\mathbf{u})]$, rescaled using the sample variances, plotted on a normal qq-plot. (b) The squared Mahalanobis distance of $\hat{P}_X^{(2)}(\epsilon, m; T, \mathbf{u})$ to $\mathbb{E}[P_X^T(\mathbf{u})]$, calculated via the sample covariance matrix of $\hat{P}_X^{(2)}(\epsilon, m; T, \mathbf{u})$, plotted against the quantiles of a $\chi^2(3)$ random variable with 3 degrees of freedom.

For each component u_i of $\mathbf{u}$, we test the null hypothesis that $\hat{P}_X^{(2)}(\epsilon, m; T, u_i)$ follows a Gaussian distribution using a Shapiro-Wilk test. The resulting p-values from the tests are 0.43, 0.65, and 0.53 respectively. Thus, the hypothesis of Gaussianity cannot be rejected for any margin of $\hat{P}_X^{(2)}(\epsilon, m; T, \mathbf{u})$. Using the R package `mvnormtest`, we test the null hypothesis that $\hat{P}_X^{(2)}(\epsilon, m; T, \mathbf{u})$ follows a multivariate normal distribution with a multivariate Shapiro-Wilk test. The test statistic corresponds to a p-value of 0.54, hence, multivariate normality cannot be rejected.

4.3. *Convergence in mean in the anisotropic case.* Assumptions 1, 2, and 3 do not restrict anisotropy. Therefore, Proposition 1 holds for anisotropic random fields. In the simulation studies that follow, it will be useful to have the theoretical value of $\mathbb{E}[P_X^T(u)]$, which is computed for X in a particular class of anisotropic random fields exhibiting so-called geometric anisotropy.

PROPOSITION 3. *Let X be a stationary, Gaussian random field defined on $\mathbb{R}^2$, with zero-mean, unit-variance, and covariance function $R(h) = \exp(-||Ah||_2^2)$, where A is a 2×2 non-singular matrix and $h \in \mathbb{R}^2$. Without loss of generality, let*

$$A = \begin{bmatrix} \sigma_1 \cos\theta & \sigma_1 \sin\theta \\ -\sigma_2 \sin\theta & \sigma_2 \cos\theta \end{bmatrix},$$

so that $\sigma_1 > 0$ and $\sigma_2 > 0$ correspond to the singular values of A, and $\theta \in [0, \pi)$ is an angle of rotation. Fix $T = [-t, t]^2$, where $t \in \mathbb{R}^+$. Then,

$$\mathbb{E}[P_X^T(u)] = \frac{\sqrt{2}}{\pi} t^2 \, \text{ellipse}(\sigma_1, \sigma_2) \, e^{-u^2/2},$$

for all $u \in \mathbb{R}$, where $\text{ellipse}(\sigma_1, \sigma_2)$ is the perimeter of an ellipse with semi-minor and semi-major axes σ_1 and σ_2.

The proof of Proposition 3 can be found in Section 5. Let us specify the anisotropic fields used in this simulation study.

EXAMPLE 2. Let $X(\cdot;\theta)$ be a stationary random field with centered Gaussian margins, and covariance function given by $R_\theta(h) := \exp(-||A_\theta h||_2^2)$ for $h \in \mathbb{R}^2$, where

$$A_\theta := \begin{bmatrix} 2 & 0 \\ 0 & 0.5 \end{bmatrix} \begin{bmatrix} \cos\theta & \sin\theta \\ -\sin\theta & \cos\theta \end{bmatrix}. \tag{11}$$

We use the R package `RandomFields` to generate these random fields in $T = [-2.5, 2.5]^2$ on a rectangular grid of size 256×256 pixels. With ϵ denoting the resulting pixel width, we wish to compare the performances of the estimators $\frac{\pi}{4}\hat{P}^{(1)}_{X(\cdot;\theta)}(\epsilon;T,u)$, $\hat{P}^{(2)}_{X(\cdot;\theta)}(\epsilon,m;T,u)$ with $m = 8$, and $\tilde{P}_{X(\cdot;\theta)}(\epsilon;T,u)$, for $u = 0.5$.
For each value of θ that is tested in $[0, \frac{\pi}{2}]$, 500 independent replications of X are simulated in the domain T and the mean of the estimates of $P^T_{X(\cdot;\theta)}(0.5)$ is plotted for each of the three estimators $\frac{\pi}{4}\hat{P}^{(1)}_{X(\cdot;\theta)}(\epsilon;T,0.5)$ (shown in green), $\hat{P}^{(2)}_{X(\cdot;\theta)}(\epsilon,8;T,0.5)$ (shown in blue), and $\tilde{P}_{X(\cdot;\theta)}(\epsilon;T,0.5)$ (shown in black) in Figure 8 (c). Notice that $\mathbb{E}\big[\frac{\pi}{4}\hat{P}^{(1)}_{X(\cdot;\theta)}(\epsilon;T,0.5)\big]$ clearly depends on θ, whereas $\mathbb{E}\big[P^T_{X(\cdot;\theta)}(0.5)\big]$ (shown in red) does not, by Proposition 3. The performance of $\hat{P}^{(2)}_{X(\cdot;\theta)}(\epsilon,8;T,0.5)$ is comparable to that of $\tilde{P}_{X(\cdot;\theta)}(\epsilon;T,0.5)$, which is interesting since the the latter estimator has access to the values of $X(\cdot;\theta)$ evaluated on the square grid $\mathcal{G}^{(T,\epsilon)}$, defined in (5); the former only has access to the binary matrix $\zeta^{(T,\epsilon)}_{X(\cdot;\theta)}(0.5)$, defined in (6).

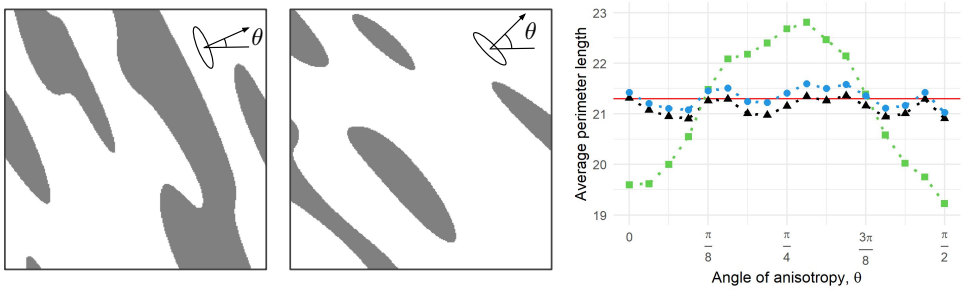

(a) $\theta = \frac{\pi}{8}$ (b) $\theta = \frac{\pi}{4}$ (c)

Fig 8: Illustration of the effect of anisotropy on estimation. The anisotropic random field $X(\cdot;\theta)$ is described in Example 2. Here, $T = [-2.5, 2.5]^2$ and $\epsilon = 5/256$. (a, b) A realization of $E_{X(\cdot;\theta)}(T, 0.5)$ shown as the dark region. The matrix A_θ, defined in (11), maps the drawn ellipse to a circle. (c) For several $\theta \in [0, \frac{\pi}{2}]$, 500 independent realizations of $X(\cdot;\theta)$ are simulated, and the mean values of $\frac{\pi}{4}\hat{P}^{(1)}_{X(\cdot;\theta)}(\epsilon;T,0.5)$ (green squares), $\hat{P}^{(2)}_{X(\cdot;\theta)}(\epsilon,8;T,0.5)$ (blue circles), and $\tilde{P}_{X(\cdot;\theta)}(\epsilon;T,0.5)$ (black triangles) are plotted. The mean estimates are shown in comparison with $\mathbb{E}\big[P^T_{X(\cdot;\theta)}(0.5)\big] = 21.3$ (red reference line, computed via Proposition 3).

In addition, we repeat the experiment in Section 4.1 for the random field $X(\cdot;\theta)$ given in Example 2. The results of the simulation study are summarised in Figure 9.

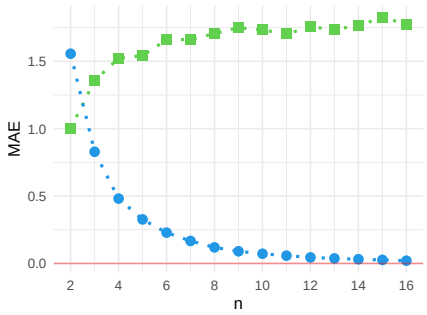

Fig 9: For the anisotropic random field $X(\cdot;\theta)$ in Example 2 with $\theta = 0$, $\tilde{P}_{X(\cdot;0)}(\epsilon_n; T, 0.5)$ is approximated by $\frac{\pi}{4}\hat{P}^{(1)}_{X(\cdot;0)}(\epsilon_n; T, 0.5)$ (green squares) and by $\hat{P}^{(2)}_{X(\cdot;0)}(\epsilon_n, m_n; T, 0.5)$ (blue circles). Here, $T = [-2.5, 2.5]^2$ and M_n, m_n, and ϵ_n are given in (9). For each n, the MAE of the approximations are calculated from 500 independent replications of the process $X(\cdot;0)$. In this simulation study, $\mathbb{E}[P^T_{X(\cdot;0)}(0.5)] = 21.3$ (computed via Proposition 3).

4.4. *Hyperparameter selection.* In practice, sampling locations often have a fixed spacing, and it is not possible to further decrease the grid spacing in the discretization. In these cases, the pixel width ϵ is a feature of the data, and so to use $\hat{P}^{(2)}_X(\epsilon, m; T, u)$, the hyperparameter m must be chosen appropriately. As a rule-of-thumb, empirical studies suggest that it is reasonable to choose

$$m = m^T_X := \lfloor C\epsilon^{-2/3} \rfloor, \tag{12}$$

with

$$C := \left(\frac{\min\left\{ \nu\big(E_X(T,u)\big),\ \nu\big(T \setminus E_X(u)\big) \right\}}{N_{cc} + N_{holes}} \right)^{1/2},$$

where N_{cc} (resp. N_{holes}) corresponds to the number of connected components (resp. holes) of $E_X(T,u)$. For a sequence $(\epsilon_n)_{n\geq 1}$ tending to 0, the corresponding sequence $(m_n)_{n\geq 1}$ determined by (12) satisfies the asymptotic relationship required by Theorem 1.

REMARK 6. In practice, $\nu\big(E_X(T,u)\big)$ and $\nu\big(T \setminus E_X(u)\big)$ can be approximated by the number of 1's and the number of 0's in $\zeta^{(T,\epsilon)}_X(u)$, rescaled by a factor of ϵ^2. The quantities N_{cc} and N_{holes} can be estimated by considering the sites in $\mathcal{G}^{(T,\epsilon)}$ to be either 4-connected or 8-connected, and colouring each site based on its corresponding value in $\zeta^{(T,\epsilon)}_X(u)$.

Figures 10 and 11 showcase the performance of $\hat{P}^{(2)}_X(\epsilon, m^T_X; T, 0)$, with m^T_X as in (12), for two different levels of discretization of the random field in Example 1.

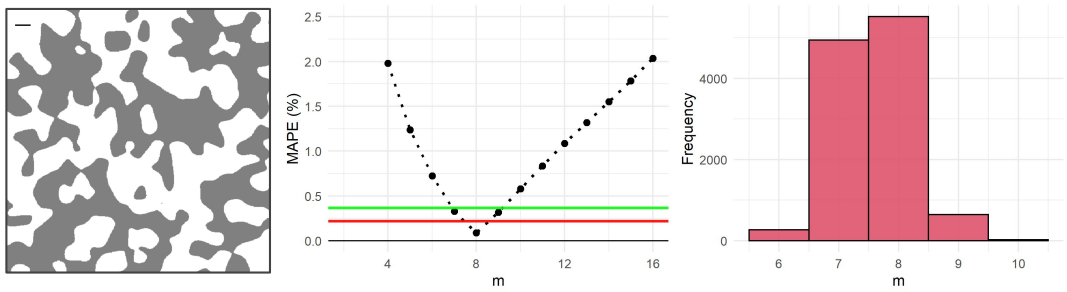

(a) (b) (c)

Fig 10: Illustration of the influence of the hyperparameter m. The mean absolute percentage error (MAPE) of several perimeter estimators is calculated for 10000 independent replications of the isotropic, Gaussian random field X in Example 1, with $T = [-10, 10]^2$, $u = 0$, and $\epsilon = 20/512$. The proxy $\tilde{P}_X(\epsilon; T, 0)$ is used to represent the true perimeter $P_X^T(0)$ for each sample path. (a) One particular realisation of $E_X(0)$ is depicted in T. Shown for scale in the top-left of the image is a line segment with length 30ϵ. (b) The points plotted in black correspond to the MAPE of $\hat{P}_X^{(2)}(\epsilon, m; T, 0)$ for various values of m. The green horizontal line (0.36%) corresponds to the MAPE of $\frac{\pi}{4}\hat{P}_X^{(1)}(\epsilon; T, 0)$, which obviously does not depend on m. The red horizontal line (0.22%) corresponds to the MAPE of $\hat{P}_X^{(2)}(\epsilon, m_X^T; T, 0)$, with m_X^T as in (12). (c) The values of m_X^T computed from the 10000 independent replications of X.

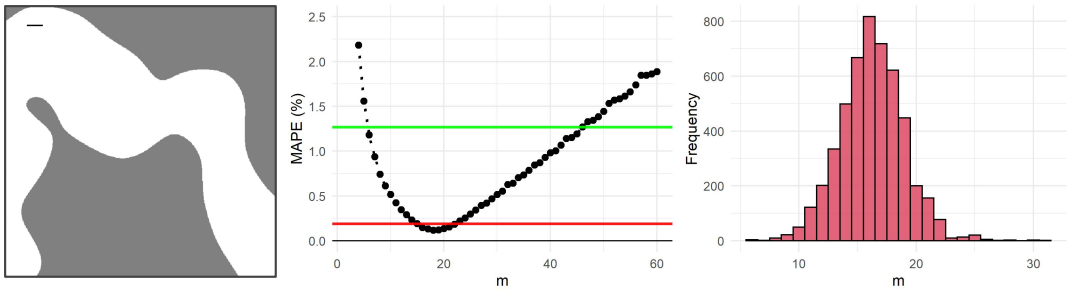

(a) (b) (c)

Fig 11: See Figure 10 for a description of the figures. In this case, $T = [-2.5, 2.5]^2$ and $\epsilon = 5/512$. The MAPE of $\frac{\pi}{4}\hat{P}_X^{(1)}(\epsilon; T, 0)$ is 1.27%, and that of $\hat{P}_X^{(2)}(\epsilon, m_X^T; T, 0)$ is 0.19%.

4.5. *Behaviour of the perimeter estimator as a function of the level u.* Dfferently from our previous numerical studies, we illustrate the behaviour of $\hat{P}_X^{(2)}(\epsilon, m_X^T; T, u)$ as a function of the level u in Figures 12 and 13.

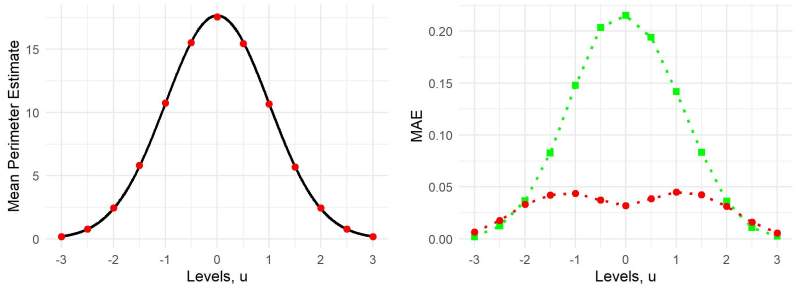

(a) (b)

Fig 12: Illustration of perimeter estimation for multiple levels. The isotropic, Gaussian random field X in Example 1 is considered on $T = [-2.5, 2.5]^2$ with a discretization of $\epsilon = 5/512$. (a) The sample mean of 1000 independent replications of $\hat{P}_X^{(2)}(\epsilon, m_X^T; T, u)$ plotted in red for several values of u, shown against $\mathbb{E}[P_X^T(u)]$ in black (computed via Adler and Taylor (2007, Theorem 15.9.5)). (b) The MAE of the approximation of $\tilde{P}_X(\epsilon; T, u)$ by $\hat{P}_X^{(2)}(\epsilon, m_X^T; T, u)$ (red circles) and $\frac{\pi}{4}\hat{P}_X^{(1)}(\epsilon, ; T, u)$ (green squares).

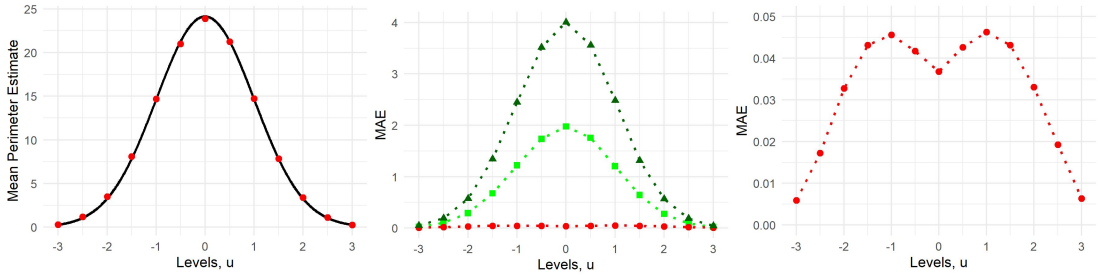

(a) (b) (c)

Fig 13: The same experiment as depicted in Figure 12, but using the anisotropic, Gaussian random field $X := X(\cdot; 0)$ in Example 2. (a) Now, $\mathbb{E}[P_X^T(u)]$, shown in black, is calculated via Proposition 3. (b) The MAE of the approximation of $\tilde{P}_X(\epsilon; T, u)$ by $\hat{P}_X^{(2)}(\epsilon, m_X^T; T, u)$ (red circles), $\frac{\pi}{4}\hat{P}_X^{(1)}(\epsilon, ; T, u)$ (green squares), and $\hat{P}_X^{(1)}(\epsilon, ; T, u)$ (dark green triangles). (c) The MAE associated to $\hat{P}_X^{(2)}(\epsilon, m_X^T; T, u)$ shown again on a more appropriate scale.

5. Proofs. This section provides a detailed justification for the theoretical results stated thus far. The following definition is used throughout this section.

DEFINITION 6. For $s \in \mathbb{R}^2$, define the set $B_s^{(l)} := [0, l)^2 + s$, where " $+$ " in this context denotes the Minkowski sum. Let $\epsilon > 0$ and $m \in \mathbb{N}^+$. Define

$$\mathcal{V}_X^T(\epsilon, m; u) := \{s_{i,j} \in \mathcal{G}^{(T,\epsilon)} : i, j \in I^{(T,\epsilon,m)},\ B_{s_{i,j}}^{(m\epsilon)} \cap E_X^{\partial}(T, u) \neq \emptyset\}.$$

The following lemma allows us to bound $\#\big(\mathcal{V}_X^T(\epsilon, m; u)\big)$, which amounts to an upper bound on the number of nonzero terms in the sum given by Equation (7). See Figure 15 in the appendix for an illustration that complements Lemma 2.

LEMMA 2. *Let X be a random field satisfying Assumption 1. For any $\epsilon > 0$ and $m \in \mathbb{N}^+$,*

$$\#\big(\mathcal{V}_X^T(\epsilon, m; u)\big) \le 4\Big(\frac{P_X^T(u)}{m\epsilon} + \#\big(\Gamma_X^T(u)\big)\Big), \qquad a.s.$$

PROOF. The squares of side length $m\epsilon$ in the set $\mathcal{B} := \{B_{s_{i,j}}^{(m\epsilon)} : i, j \in I^{(T,\epsilon,m)}\}$ are disjoint and cover T. For each $\gamma \in \Gamma_X^T(u)$, it is possible to find connected subsets of γ, namely $\beta_{\gamma,1}$, $\ldots$, β_{γ,M_γ}, that satisfy

$$\gamma = \bigcup_{i=1}^{M_\gamma} \beta_{\gamma,i},$$

where

$$M_\gamma := \Big\lfloor \frac{\mathcal{H}^1(\gamma)}{m\epsilon} \Big\rfloor + 1,$$

and for all $i \in \{1, \ldots, M_\gamma\}$,

$$\mathcal{H}^1(\beta_{\gamma,i}) \le m\epsilon.$$

Each $\beta_{\gamma,i}$ can intersect at most 4 elements of $\mathcal{B}$. Since

$$E_X^\partial(T, u) = \bigcup_{\gamma \in \Gamma_X^T(u)} \bigcup_{i=1}^{M_\gamma} \beta_{\gamma,i},$$

it follows that

$$\begin{aligned}\#\big(\mathcal{V}_X^T(\epsilon, m; u)\big) &= \#\big(\{b \in \mathcal{B} : b \cap E_X^\partial(T, u) \neq \emptyset\}\big) \\ &\le 4 \sum_{\gamma \in \Gamma_X^T(u)} M_\gamma \le 4\Big(\frac{P_X^T(u)}{m\epsilon} + \#\big(\Gamma_X^T(u)\big)\Big), \qquad a.s.\end{aligned}$$

□

PROOF OF THEOREM 1. Let $\omega \in \Omega$ be such that $\Lambda_{X(\omega)}^T(u)$, defined in Definition 5, is positive (note that almost any $\omega \in \Omega$ will suffice, as discussed in Remark 4). There exists $n_0 \in \mathbb{N}^+$ such that $E_{X(\omega)}(u)$ is resolved by $m_n\epsilon_n$ in T for all $n \ge n_0$ (see Definition 5). Fix $s_{i,j} \in \mathcal{V}_{X(\omega)}^T(\epsilon_n, m_n; u)$ and $n \ge n_0$. Let $\gamma := B_{s_{i,j}}^{(m_n\epsilon_n)} \cap E_{X(\omega)}^\partial(T, u)$. It follows from our construction that $\mathcal{Y}_{X(\omega)}^T(u) \cap \gamma$ contains at most one element, since the spacing between points in $\mathcal{Y}_{X(\omega)}^T(u)$ is larger than the diameter of $B_{s_{i,j}}^{(m_n\epsilon_n)}$. It also follows from our construction that γ is either connected, or the union of two maximally connected subsets. To see this, note that the planar curvature of γ does not exceed $1/(m_{n_0}\epsilon_{n_0})$ since $m_{n_0}\epsilon_{n_0}$ is smaller than the reach of both $E_{X(\omega)}(T, u)$ and $T \setminus E_{X(\omega)}(u)$. Therefore, the curve is bounded by the planar arcs of radius $m_{n_0}\epsilon_{n_0}$ as shown in Figure 14 (see Dubins (1961)). We aim to bound the absolute difference between the length of γ and its contribution to $\hat{P}_{X(\omega)}^{(2)}(\epsilon_n, m_n; T, u)$. To this end, the two cases are shown in Figure 14 separately.

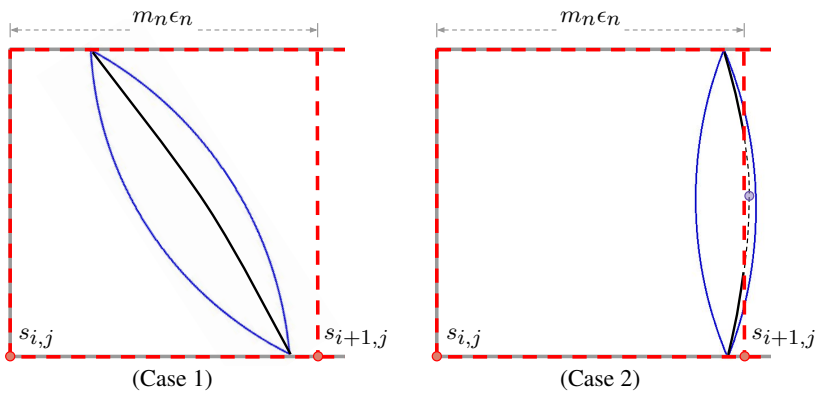

Fig 14: (Case 1) The curve γ shown in black is bounded by the planar arcs of radius $m_{n_0}\epsilon_{n_0}$ shown in blue. (Case 2) Here, γ shown in black is not connected, and the only point in $\mathcal{Y}^T_{X(\omega)}(u) \cap B^{(m_n\epsilon_n)}_{s_{i+1,j}}$ is highlighted in purple.

Case 1: *The curve γ is connected (see the left panel of Figure 14).* The closure of γ can be parameterized by a continuous injective vector function $\mathbf{x} : [0,1] \to \mathbb{R}^2$. For $\alpha \in [0,1]$, define

$$\mathrm{TV}_k(\alpha; s_{i,j}) := \int_0^\alpha |x_k'(s)| \, \mathrm{d}s, \qquad k \in \{1,2\}, \tag{13}$$

so that $\mathrm{TV}_k(1; s_{i,j})$ corresponds to the total variation of γ in the k^{th} principle Cartesian direction of $\mathbb{R}^2$. As a consequence of the coarea formula (Adler and Taylor, 2007, Equation (7.4.15)), the quantity $\epsilon_n N_{X(\omega),h}(i,j;u)$ (see Definition 4) is a Riemann sum that approximates the definite integral $\mathrm{TV}_1(1; s_{i,j})$. The total error can therefore be bounded above by

$$\left|\epsilon_n N_{X(\omega),h}(i,j;u) - \mathrm{TV}_1(1; s_{i,j})\right| \leq 4\epsilon_n, \tag{14}$$

as suggested by Figure 16, found in the appendix. Analogously,

$$\left|\epsilon_n N_{X(\omega),v}(i,j;u) - \mathrm{TV}_2(1; s_{i,j})\right| \leq 4\epsilon_n.$$

Let

$$\hat{l}_n(s_{i,j}) := \epsilon_n \left|\left|\left(N_{X(\omega),v}(i,j;u), N_{X(\omega),h}(i,j;u)\right)\right|\right|_2, \tag{15}$$

and we achieve the following bound by the triangle inequality

$$\left|\hat{l}_n(s_{i,j}) - \left|\left|\left(\mathrm{TV}_1(1; s_{i,j}), \mathrm{TV}_2(1; s_{i,j})\right)\right|\right|_2\right| \leq 4\sqrt{2}\epsilon_n. \tag{16}$$

It is clear that

$$||\mathbf{x}(1) - \mathbf{x}(0)||_2 \leq \left|\left|\left(\mathrm{TV}_1(1; s_{i,j}), \mathrm{TV}_2(1; s_{i,j})\right)\right|\right|_2, \tag{17}$$

since the computation of the left-hand side of Equation (17) involves the same integral as in (13) but without the absolute values. In addition, let

$$l(\alpha; s_{i,j}) := \int_0^\alpha ||\mathbf{x}'(s)||_2 \, \mathrm{d}s$$

denote the length of $\mathbf{x}(s)$ for $s \in [0,\alpha]$. It follows from the definition of the derivative and the reverse triangle inequality that for all $\alpha \in (0,1)$,

$$\left|\frac{\partial}{\partial\alpha}\left|\left|\left(\mathrm{TV}_1(\alpha; s_{i,j}), \mathrm{TV}_2(\alpha; s_{i,j})\right)\right|\right|_2\right| \leq \left|\left|\left(x_1'(\alpha), x_2'(\alpha)\right)\right|\right|_2 = \frac{\partial}{\partial\alpha} l(\alpha; s_{i,j}).$$

Therefore,

$$\left|\left|\left(\mathrm{TV}_1(1;s_{i,j}),\mathrm{TV}_2(1;s_{i,j})\right)\right|\right|_2 \le l(1;s_{i,j}). \tag{18}$$

Since the curvature of γ is bounded above by the inverse of $\Lambda^T_{X(\omega)}(u)$, we apply a well known result from Schwartz (see Dubins (1961)) that guarantees that

$$l(1;s_{i,j}) \le a(s_{i,j}), \tag{19}$$

where $a(s_{i,j})$ is the length of the smallest planar arc with radius $m_{n_0}\epsilon_{n_0}$ that has endpoints $\mathbf{x}(0)$ and $\mathbf{x}(1)$. The Taylor expansion of the sine function shows the existence of $K \in \mathbb{R}^+$ independent of $s_{i,j}$ and n such that

$$\left|a(s_{i,j}) - ||\mathbf{x}(1)-\mathbf{x}(0)||_2\right| \le K||\mathbf{x}(1)-\mathbf{x}(0)||_2^3 \le K(\sqrt{2}m_n\epsilon_n)^3. \tag{20}$$

Assembling the bounds demonstrated in Equations (17), (18), and (19), we get

$$||\mathbf{x}(1)-\mathbf{x}(0)||_2 \le \left|\left|\left(\mathrm{TV}_1(1;s_{i,j}),\mathrm{TV}_2(1;s_{i,j})\right)\right|\right|_2 \le l(1;s_{i,j}) \le a(s_{i,j}),$$

which in combination with (20) implies

$$\left|l(1;s_{i,j}) - \left|\left|\left(\mathrm{TV}_1(1;s_{i,j}),\mathrm{TV}_2(1;s_{i,j})\right)\right|\right|_2\right| \le K(\sqrt{2}m_n\epsilon_n)^3. \tag{21}$$

Now, combining Equations (21) and (16) by the triangle inequality yields

$$\left|\hat{l}_n(s_{i,j}) - l(1;s_{i,j})\right| \le K(\sqrt{2}m_n\epsilon_n)^3 + 4\sqrt{2}\epsilon_n. \tag{22}$$

Case 2: *The curve γ has two connected components (see the right panel of Figure 14).* Similarly to Case 1, we parameterize the closure of each maximally connected subset of γ with continuous injective vector functions $\mathbf{x} : [0,1] \to \mathbb{R}^2$ and $\mathbf{y} : [0,1] \to \mathbb{R}^2$. For $\alpha \in [0,1]$, define

$$\mathrm{TV}_k(\alpha;s_{i,j}) := \int_0^\alpha \left(|x_k'(s)| + |y_k'(s)|\right)\,\mathrm{d}s, \qquad k \in \{1,2\}.$$

With $\hat{l}_n(s_{i,j})$ defined as in (15), Equation (16) holds. Now, consider the curve $\tilde{\gamma} := (B^{(m_n\epsilon_n)}_{s_{i,j}} \cup B^{(m_n\epsilon_n)}_{s_{i+1,j}}) \cap E^{\partial}_{X(\omega)}(T,u)$, which is γ in union with the middle section in the adjacent box $B^{(m_n\epsilon_n)}_{s_{i+1,j}}$ (where we have assumed, without loss of generality, that the "middle section" is in the box to the right). It is clear that $\tilde{\gamma}$ is connected, so its closure can be parameterized by the continuous injective vector function $\mathbf{z} : [0,1] \to \mathbb{R}^2$. Define

$$\widetilde{\mathrm{TV}}_k(\alpha;s_{i,j}) := \int_0^\alpha |z_k'(s)|\,\mathrm{d}s, \qquad k \in \{1,2\}$$

and

$$\tilde{l}(\alpha;s_{i,j}) := \int_0^\alpha ||z'(s)||_2\,\mathrm{d}s.$$

By the same arguments that led to Equation (21), it holds that

$$0 \le \tilde{l}(1;s_{i,j}) - \left|\left|\left(\widetilde{\mathrm{TV}}_1(1;s_{i,j}),\widetilde{\mathrm{TV}}_2(1;s_{i,j})\right)\right|\right|_2 \le K(\sqrt{2}m_n\epsilon_n)^3, \tag{23}$$

where $K \in \mathbb{R}^+$ is independent of $s_{i,j}$ and n. Let

$$l(1;s_{i,j}) := \int_0^1 \left(||\mathbf{x}'(s)||_2 + ||\mathbf{y}'(s)||_2\right)\,\mathrm{d}s$$

be the total length of γ. Then $\tilde{l}(1;s_{i,j}) = l(1;s_{i,j}) + l(1;s_{i+1,j})$, and

$$\left|\left|\left(\widetilde{\mathrm{TV}_1}(1;s_{i,j}), \widetilde{\mathrm{TV}_2}(1;s_{i,j})\right)\right|\right|_2 \leq \left|\left|\left(\mathrm{TV}_1(1;s_{i,j}), \mathrm{TV}_2(1;s_{i,j})\right)\right|\right|_2 + \left|\left|\left(\mathrm{TV}_1(1;s_{i+1,j}), \mathrm{TV}_2(1;s_{i+1,j})\right)\right|\right|_2$$

by the triangle inequality. Therefore, (23) can be written as

$$\begin{aligned}&\left(l(1;s_{i,j}) - \left|\left|\left(\mathrm{TV}_1(1;s_{i,j}), \mathrm{TV}_2(1;s_{i,j})\right)\right|\right|_2\right) + \\ &\left(l(1;s_{i+1,j}) - \left|\left|\left(\mathrm{TV}_1(1;s_{i+1,j}), \mathrm{TV}_2(1;s_{i+1,j})\right)\right|\right|_2\right) \leq K(\sqrt{2}m_n\epsilon_n)^3. \end{aligned} \tag{24}$$

By the arguments in Case 1 that led to Equation (18), it follows that

$$l(1;s_{i+1,j}) \geq \left|\left|\left(\mathrm{TV}_1(1;s_{i+1,j}), \mathrm{TV}_2(1;s_{i+1,j})\right)\right|\right|_2,$$

and by the same arguments,

$$l(1;s_{i,j}) \geq \left|\left|\left(\mathrm{TV}_1(1;s_{i,j}), \mathrm{TV}_2(1;s_{i,j})\right)\right|\right|_2.$$

Therefore, both (21) and (22) follow from Equation (24).

Following from Equation (22), we have

$$\begin{aligned}\left|\hat{P}^{(2)}_{X(\omega)}(\epsilon_n, m_n; T, u) - P^T_{X(\omega)}(u)\right| &= \left|\sum_{s_{i,j} \in \mathcal{V}^T_{X(\omega)}(\epsilon_n, m_n; u)} \left(\hat{l}_n(s_{i,j}) - l(1;s_{i,j})\right)\right| \\ &\leq \sum_{s_{i,j} \in \mathcal{V}^T_{X(\omega)}(\epsilon_n, m_n; u)} \left|\hat{l}_n(s_{i,j}) - l(1;s_{i,j})\right| \\ &\leq \#\left(\mathcal{V}^T_{X(\omega)}(\epsilon_n, m_n; u)\right) 2\sqrt{2}(Km_n^3\epsilon_n^3 + 2\epsilon_n).\end{aligned}$$

By Lemma 2,

$$\begin{aligned}&g_n\left|\hat{P}^{(2)}_{X(\omega)}(\epsilon_n, m_n; T, u) - P^T_{X(\omega)}(u)\right| \\ &\qquad \leq 8\sqrt{2}g_n\left(\frac{P^T_{X(\omega)}(u)}{m_n\epsilon_n} + \#\left(\Gamma^T_{X(\omega)}(u)\right)\right)\left(Km_n^3\epsilon_n^3 + 2\epsilon_n\right) \\ &\qquad = 8\sqrt{2}\,\frac{g_n}{m_n}\left(P^T_{X(\omega)}(u) + m_n\epsilon_n \#\left(\Gamma^T_{X(\omega)}(u)\right)\right)\left(Km_n^3\epsilon_n^2 + 2\right), \end{aligned} \tag{25}$$

which tends to 0 as $n \to \infty$. This convergence holds for almost every $\omega \in \Omega$, since $\Lambda^T_X(u)$ is almost surely positive. □

PROOF OF COROLLARY 1. The last expression in Equation (25) tends to 0 under the relaxed constraint on $(\epsilon_n)_{n\geq 1}$ if $g_n = 1$ for all $n \in \mathbb{N}^+$. □

PROOF OF PROPOSITION 1. If a sequence is uniformly integrable, convergence in $L^1(\Omega)$ is equivalent to convergence in probability. Therefore, by Corollary 1, it suffices to show that $\left(\hat{P}^{(2)}_X(\epsilon_n, m_n; T, u)\right)_{n\geq 1}$ is bounded above by an element of $L^1(\Omega)$ uniformly in n. Note that for each $n \geq 1$,

$$\hat{P}^{(2)}_X(\epsilon_n, m_n; T, u) \leq \hat{P}^{(1)}_X(\epsilon_n; T, u), \qquad a.s.$$

since the 2-norm is inferior to the 1-norm. Now, consider the quantity

$$G_n = \#\left(\left\{s \in \mathcal{G}^{(T,\epsilon_n)} : B^{(\epsilon_n)}_s \cap E^{\partial}_X(T,u) \neq \emptyset\right\}\right),$$

which represents the number of pixels of side length ϵ_n that the curve $E_X^{\partial}(T,u)$ intersects. Almost surely, $\hat{P}_X^{(1)}(\epsilon_n;T,u)$ is at most ϵ_n times the number of pixel edges that intersect $E_X^{\partial}(T,u)$, and there are at most $4G_n$ such pixel edges. By the same arguments used to prove Lemma 2, we have for all $n \geq 1$,

$$G_n \leq 4\Big(\frac{P_X^T(u)}{\epsilon_n} + \#\big(\Gamma_X^T(u)\big)\Big), \qquad a.s.$$

and

$$\hat{P}_X^{(2)}(\epsilon_n, m_n; T, u) \leq \hat{P}_X^{(1)}(\epsilon_n; T, u) \leq 4G_n\epsilon_n \leq 16\Big(P_X^T(u) + \sup_n(\epsilon_n)\#\big(\Gamma_X^T(u)\big)\Big), \qquad a.s.$$

which is in $L^1(\Omega)$ by Assumption 3. □

PROOF OF LEMMA 1. It is clear that Assumption 4 implies Assumption 1. Under Assumption 4, Theorem 11.3.3 of Adler and Taylor (2007) implies that X is almost surely *suitably regular* (Adler and Taylor, 2007, Definition 6.2.1) over bounded rectangles, which together with the assumption of isotropy implies the conditions of Assumption 2. The expectations of $P_X^{T_n}(u)$ and $\#\big(\Gamma_X^{T_n}(u)\big)$ are shown in Kratz and Vadlamani (2018) and Beliaev, McAuley and Muirhead (2020) respectively to be $O\big(\nu(T_n)\big)$; therefore, they are finite for all $n \in \mathbb{N}^+$, implying the conditions of Assumption 3. □

PROOF OF PROPOSITION 2. Let

$$W_n := \frac{\hat{P}_X^{(2)}(\epsilon_n, m_n; T_n, u) - P_X^{T_n}(u)}{\sqrt{\nu(T_n)}}.$$

Given that $E_X(u)$ is resolved by $m_n\epsilon_n$ in T_n for fixed $n \in \mathbb{N}^+$, Equation (25) holds with $g_n = 1/\sqrt{\nu(T_n)}$, implying

$$\begin{aligned} |W_n| &\leq \frac{8}{m_n}\sqrt{\frac{2}{\nu(T_n)}}\Big(P_X^{T_n}(u) + m_n\epsilon_n\#\big(\Gamma_X^{T_n}(u)\big)\Big)\Big(Km_n^3\epsilon_n^2 + 2\Big) \\ &= \frac{8\sqrt{2\nu(T_n)}}{m_n}\left(\frac{P_X^{T_n}(u)}{\nu(T_n)} + m_n\epsilon_n\frac{\#\big(\Gamma_X^{T_n}(u)\big)}{\nu(T_n)}\right)\Big(Km_n^3\epsilon_n^2 + 2\Big), \end{aligned} \tag{26}$$

where $K \in \mathbb{R}^+$ is independent of n. As discussed in the proof of Lemma 1, both

$$\limsup_{n\to\infty}\frac{P_X^{T_n}(u)}{\nu(T_n)} \qquad \text{and} \qquad \limsup_{n\to\infty}\frac{\#\big(\Gamma_X^{T_n}(u)\big)}{\nu(T_n)}$$

are finite almost surely. Thus, the final expression in (26) tends to 0 almost surely, since $\sqrt{\nu(T_n)}/m_n \to 0$ by assumption. Now, denote the random event $A_n := \{m_n\epsilon_n < \Lambda_X^{T_n}(u)\}$, and let A_n^C denote its complement. Since $\mathbb{P}(A_n) \to 1$ as $n \to \infty$ by assumption, it holds that for any $\eta > 0$,

$$\mathbb{P}(|W_n| > \eta) \leq \mathbb{P}(|W_n| > \eta \mid A_n)\mathbb{P}(A_n) + \mathbb{P}(A_n^C) \to 0$$

as $n \to \infty$. □

PROOF OF THEOREM 2. Recall from Kratz and Vadlamani (2018) that the Lipschitz-Killing curvatures of the excursion sets of isotropic random fields satisfying Assumption 4 follow a multivariate central limit theorem, as proven earlier in Kratz and León (2001) for the perimeter of two-dimensional excursions. The result is proven for a single level u, but as noted in the

Discussion of Kratz and Vadlamani (2018) and in Shashkin (2013) the Cramér-Wald device can be used to extend the arguments to the multivariate setting. Moreover, it is noted in both Kratz and León (2001) and Kratz and Vadlamani (2018, Remark 3.4) that the assumption of isotropy can be relaxed, and the result still holds. The central limit theorem for the perimeter is then written as follows. For any $\mathbf{u} \in \mathbb{R}^k$ satisfying the given constraints, it holds that

$$\frac{P_X^{T_n}(\mathbf{u}) - \mathbb{E}[P_X^{T_n}(\mathbf{u})]}{\sqrt{\nu(T_n)}} \xrightarrow{\mathrm{d}} \mathcal{N}_k\big(\mathbf{0}, \Sigma(\mathbf{u})\big), \qquad n \to \infty. \tag{27}$$

The proof of our Theorem 2 is finished by combining Equation (27), Proposition 2, and Slutsky's theorem. □

PROOF OF PROPOSITION 3. Let Y be a random field defined on $\mathbb{R}^2$ that satisfies $Y(s) = X(A^{-1}s)$ almost surely for all $s \in \mathbb{R}^2$. It follows that Y is isotropic, and so we can apply the kinematic formula in Theorem 15.9.5 of Adler and Taylor (2007) as is done in Section 2.2 of Biermé et al. (2019) to obtain

$$\mathbb{E}[P_Y^T(u)] = \frac{(2t)^2}{\sqrt{2}} e^{-u^2/2},$$

for all $u \in \mathbb{R}$. Let D be a closed disk contained in T, and define $\gamma = E_Y^{\partial}(D, u)$. Then

$$\frac{\mathbb{E}[\mathcal{H}^1(\gamma)]}{\nu(D)} = \frac{\mathbb{E}[P_Y^T(u)]}{\nu(T)} = \frac{e^{-u^2/2}}{\sqrt{2}}.$$

By the Crofton formula (see, *e.g.*, Equation (13.1.2) of Adler and Taylor (2007)),

$$\mathcal{H}^1(\gamma) = \frac{1}{4} \int_{-\infty}^{\infty} \int_0^{2\pi} n_\gamma(\varphi, p) \, \mathrm{d}\varphi \, \mathrm{d}p,$$

where $n_\gamma(\varphi, p)$ is the number points at which γ intersects an oriented line in $\mathbb{R}^2$ with orientation angle φ and signed distance p from the origin. Since Y is isotropic, $\mathbb{E}[n_\gamma(\varphi, p)]$ has no dependence on φ. Define $\beta = E_X^{\partial}(D, u)$. Then there exists a function $h : [0, 2\pi) \to \mathbb{R}^+$ such that

$$\mathbb{E}[n_\beta(\varphi, p)] = h(\varphi)\mathbb{E}[n_\gamma(0, p)],$$

for all $\varphi \in [0, 2\pi)$ and $p \in \mathbb{R}$. Moreover, $h(\varphi)$ is entirely determined by the matrix A, since $\partial\big(E_X(u)\big)$ is the image of $\partial\big(E_Y(u)\big)$ under the linear transform A^{-1}. It follows that

$$\begin{aligned}
\mathbb{E}[\mathcal{H}^1(\beta)] &= \frac{1}{4} \int_{-\infty}^{\infty} \int_0^{2\pi} \mathbb{E}[n_\beta(\varphi, p)] \, \mathrm{d}\varphi \, \mathrm{d}p \\
&= \left(\frac{1}{2\pi} \int_0^{2\pi} h(\varphi) \, \mathrm{d}\varphi \right) \left(\frac{2\pi}{4} \int_{-\infty}^{\infty} \mathbb{E}[n_\gamma(0, p)] \, \mathrm{d}p \right) \\
&= \left(\frac{1}{2\pi} \int_0^{2\pi} h(\varphi) \, \mathrm{d}\varphi \right) \mathbb{E}[\mathcal{H}^1(\gamma)]. \qquad (28)
\end{aligned}$$

Note that h depends only on A, so we consider another random object that also satisfies (28) to find the average value of h on $[0, 2\pi)$. Let $\mathcal{P}$ be a homogeneous point process on $\mathbb{R}^2$ with rate $\lambda \in \mathbb{R}$. For fixed $r > 0$, define

$$\Xi_r = \{s \in \mathbb{R}^2 : \exists \, p \in \mathcal{P} \text{ s.t. } ||s - p||_2 = r\}$$

to be the set of circles of radius r whose centers are the points in $\mathcal{P}$. Let $\tilde{\gamma}_r = \Xi_r \cap D$, and $\tilde{\beta}_r = (A^{-1}\Xi_r) \cap D$. It is easy to see that

$$\mathbb{E}[\mathcal{H}^1(\tilde{\gamma}_r)] = 2\pi r \, \lambda\nu(D)$$

and

$$\mathbb{E}[\mathcal{H}^1(\tilde{\beta}_r)] = \text{ellipse}(\sigma_1^{-1}r, \sigma_2^{-1}r)\ \det(A)\lambda\nu(D),$$

where $\det(A)$ denotes the determinant of A, or equivalently, the product of the singular values of A. Therefore,

$$\mathbb{E}[\mathcal{H}^1(\tilde{\beta}_r)] = \frac{\text{ellipse}(\sigma_1^{-1}r, \sigma_2^{-1}r)\sigma_1\sigma_2}{2\pi r}\mathbb{E}[\mathcal{H}^1(\tilde{\gamma}_r)] = \frac{\text{ellipse}(\sigma_1, \sigma_2)}{2\pi}\mathbb{E}[\mathcal{H}^1(\tilde{\gamma}_r)].$$

Since Equation (28) holds for $\tilde{\beta}_r$ and $\tilde{\gamma}_r$ in place of β and γ respectively, it follows that

$$\frac{1}{2\pi}\int_0^{2\pi} h(\varphi)\ \mathrm{d}\varphi = \frac{\text{ellipse}(\sigma_1, \sigma_2)}{2\pi}.$$

Finally,

$$\frac{\mathbb{E}[\mathcal{H}^1(\beta)]}{\mathbb{E}[\mathcal{H}^1(\gamma)]} = \frac{\mathbb{E}[P_X^T(u)]}{\mathbb{E}[P_Y^T(u)]} = \frac{\text{ellipse}(\sigma_1, \sigma_2)}{2\pi},$$

and so

$$\begin{aligned}\mathbb{E}[P_X^T(u)] &= \frac{\text{ellipse}(\sigma_1, \sigma_2)}{2\pi}\mathbb{E}[P_Y^T(u)] \\ &= \frac{\text{ellipse}(\sigma_1, \sigma_2)}{2\pi}\ \frac{(2t)^2}{\sqrt{2}}e^{-u^2/2} = \frac{\sqrt{2}}{\pi}t^2\ \text{ellipse}(\sigma_1, \sigma_2)\ e^{-u^2/2}.\end{aligned}$$

□

Discussion. We have shown for a large class of random fields that $\hat{P}_X^{(p)}(\epsilon, m; T, u)$ with $p = 2$ is a consistent and asymptotically normal estimator for $P_X^T(u)$. Our numerous simulation studies showcase the advantages of choosing the norm $p = 2$ as opposed to $p = 1$. For $p > 2$, we do not expect $\hat{P}_X^{(p)}(\epsilon, m; T, u)$ to have desirable properties, since there is a bias introduced for certain orientations of the curve $E_X^{\partial}(T, u)$. There is a natural extension of $\hat{P}_X^{(p)}(\epsilon, m; T, u)$ to random fields defined on $\mathbb{R}^d$, with $d > 2$, and it is plausible that analogous results hold in this multivariate setting. For example, Theorem 2 is based on the central limit theorem in Kratz and Vadlamani (2018), which holds in arbitrary dimension. Future work might also investigate the rate at which $\Lambda_X^T(u)$ tends weakly to 0 as $T \nearrow \mathbb{R}^2$, which would provide a more explicit constraint on the rate at which $\epsilon_n \to 0$ in Proposition 2.

APPENDIX

Here, we provide two figures; one to complement Lemma 2, and the other, Equation (14).

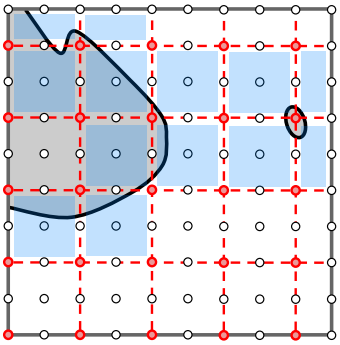

Fig 15: An illustration to aid Lemma 2. With $m = 2$, the curve $E_X^{\partial}(T, u)$ shown in black intersects 13 elements of $\{B_{s_{i,j}}^{(m\epsilon)} : i, j \in I^{(T,\epsilon,m)}\}$, which are highlighted in blue. Thus, $\#\big(\mathcal{V}_X^T(\epsilon, m; u)\big) = 13$.

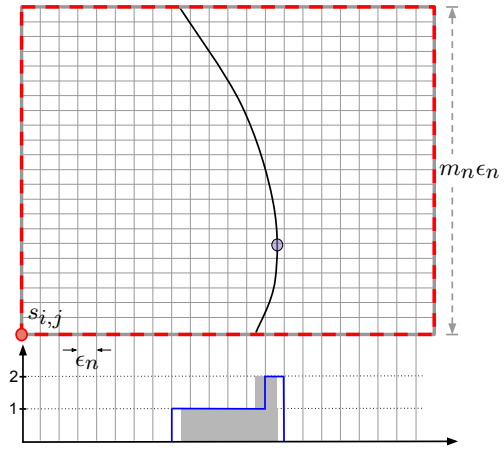

Fig 16: The approximation of $TV_1(1, s_{i,j})$ in (13) by $\epsilon_n N_{X(\omega),h}(i, j; u)$ (see Definition 4). The black curve γ is shown in $B_{s_{i,j}}^{(m_n\epsilon_n)}$, which we outline in dashed red. The definite integral $TV_1(1, s_{i,j})$ is represented by the grey area, and is approximated by $\epsilon_n N_{X(\omega),h}(i, j; u) = 7\epsilon_n$, the area under the blue curve. The absolute error of this approximation is clearly bounded above by $4\epsilon_n$ as stated in Equation (14). Highlighted in purple is a point in $\mathcal{Y}_{X(\omega)}^T(u)$ (see Equation (2)).

Acknowledgments. This work has been supported by the French government, through the 3IA Côte d'Azur Investments in the Future project managed by the National Research Agency (ANR) with the reference number ANR-19-P3IA-0002. This work has been partially supported by the project ANR MISTIC (ANR-19-CE40-0005).

REFERENCES

AAMARI, E., KIM, J., CHAZAL, F., MICHEL, B., RINALDO, A. and WASSERMAN, L. (2019). Estimating the reach of a manifold. *Electronic Journal of Statistics* **13** 1359–1399.

ABAACH, M., BIERMÉ, H. and DI BERNARDINO, E. (2021). Testing marginal symmetry of digital noise images through the perimeter of excursion sets. *Electronic Journal of Statistics* **15** 6429–6460.

ADLER, R. J. and TAYLOR, J. E. (2007). *Random fields and geometry*. *Springer Monographs in Mathematics*. Springer, New York.

ANGULO, J. and MADRID, A. (2010). Structural analysis of spatio-temporal threshold exceedances. *Environmetrics* **21** 415–438.

AZAIS, J. M. and WSCHEBOR, M. (2007). *Level Sets and Extrema of Random Processes and Fields*. John Wiley and Sons Ltd, United Kingdom.

BELIAEV, D., MCAULEY, M. and MUIRHEAD, S. (2020). On the number of excursion sets of planar Gaussian fields. *Probability Theory and Related Fields* **178** 655–698.

BERZIN, C. (2017). Estimation of Local Anisotropy Based on Level Sets. *Electronic Journal of Probability* **0** 1–72.

BIERMÉ, H. and DESOLNEUX, A. (2021). The effect of discretization on the mean geometry of a 2D random field. *Annales Henri Lebesgue* **4** 1295–1345.

BIERMÉ, H., DI BERNARDINO, E., DUVAL, C. and ESTRADE, A. (2019). Lipschitz-Killing curvatures of excursion sets for two-dimensional random fields. *Electronic Journal of Statistics* **13** 536–581.

BOLIN, D. and LINDGREN, F. (2015). Excursion and contour uncertainty regions for latent Gaussian models. *Journal of the Royal Statistical Society: Series B (Statistical Methodology)* **77** 85–106.

CABAÑA, E. M. (1987). Affine Processes: A Test of Isotropy Based on Level Sets. *SIAM Journal on Applied Mathematics* **47** 886–891.

COEURJOLLY, D. and KLETTE, R. (2004). A Comparative Evaluation of Length Estimators of Digital Curves. *IEEE transactions on pattern analysis and machine intelligence* **26** 252–8.

DE VIEILLEVILLE, F., LACHAUD, J. O. and FESCHET, F. (2007). Maximal digital straight segments and convergence of discrete geometric estimators. *Journal of Mathematical Image and Vision* **27** 471–502.

DI BERNARDINO, E. and DUVAL, C. (2020). Statistics for Gaussian random fields with unknown location and scale using Lipschitz-Killing curvatures. *Scandinavian Journal of Statistics* 1–42.

DI BERNARDINO, E., ESTRADE, A. and LEÓN, J. R. (2017). A test of Gaussianity based on the Euler characteristic of excursion sets. *Electronic Journal of Statistics* **11** 843–890.

DUBINS, L. E. (1961). On plane curves with curvature. *Pacific Journal of Mathematics* **11** 471–481.

FRÖLICHER, T. L., FISCHER, E. M. and GRUBER, N. (2018). Marine heatwaves under global warming. *Nature* **560** 360–364.

GOTT, J. R., PARK, C., JUSZKIEWICZ, R., BIES, W. E., BENNETT, D. P., BOUCHET, F. R. and STEBBINS, A. (1990). Topology of Microwave Background Fluctuations: Theory. *Astrophysical Journal* **352** 1.

KRATZ, M. and LEÓN, J. R. (2001). Central Limit Theorems for Level Functionals of Stationary Gaussian Processes and Fields. *Journal of Theoretical Probability* **14** 639–672.

KRATZ, M. and VADLAMANI, S. (2018). Central Limit Theorem for Lipschitz–Killing Curvatures of Excursion Sets of Gaussian Random Fields. *Journal of Theoretical Probability* **31** 1729–1758.

LHOTKA, O. and KYSELÝ, J. (2015). Characterizing joint effects of spatial extent, temperature magnitude and duration of heat waves and cold spells over Central Europe. *International Journal of Climatology* **35** 1232–1244.

MCGARIGAL, K. (1995). *FRAGSTATS: spatial pattern analysis program for quantifying landscape structure* **351**. US Department of Agriculture, Forest Service, Pacific Northwest Research Station.

NAGENDRA, H., MUNROE, D. K. and SOUTHWORTH, J. (2004). From pattern to process: landscape fragmentation and the analysis of land use/land cover change. *Agriculture, Ecosystems & Environment* **101** 111–115.

SHASHKIN, A. (2013). A functional central limit theorem for the level measure of a Gaussian random field. *Statistics & Probability Letters* **83** 637–643.

THÄLE, C. (2008). 50 years sets with positive reach—a survey. *Surveys in Mathematics and its Applications* **3** 123–165.

WORSLEY, K. J., EVANS, A., MARRETT, S. and NEELIN, P. (1992). A Three-Dimensional Statistical Analysis for CBF Activation Studies in Human Brain. *Journal of cerebral blood flow and metabolism : official journal of the International Society of Cerebral Blood Flow and Metabolism* **12** 900–18.